EXPERIMENTAL AND ANALYTIC STUDY OF THE DAMPED ROCKING MOVEMENT OF A CYLINDRICAL SHELL IN A FLOWING ANNULAR CHANNEL

B. Migot, A. Malon
AREVA NP, Technical Center
30 boulevard de l'Industrie, 71200, Le Creusot, FRANCE
benoit.migot@areva.com

R.J. Gibert
RJG-Conseil
44 boulevard Voltaire, 75011, Paris, FRANCE
rjgibert@orange.fr

ABSTRACT

In a general way, Pressurized Water Reactors lower internals are made up of concentric shells separated by water sheets. More exactly, in the case of the EPR™, the water sheet between the core barrel and the heavy reflector is extremely thin, providing to the fluid-structure interaction a quite particular importance. In this kind of configuration, all fluid effects must be taken into account: inertia, viscosity and mass flow. Literature provides some cases of similar studies, but usually fluid effects are investigated only for a quiescent fluid which is not the case between the core barrel and the heavy reflector (velocity ~ 1 m/s). For these reasons, an experimental analysis is conducted on a mock-up aiming at recreating the main characteristics of the problem with the simplest possible structure: a cylindrical shell favoring the first rocking mode (n=1), confined outside by a very rigid cylindrical shell to obtain vibratory variations of the fluid sheet thickness. Test facility makes possible to vary the following parameters: sheet thickness, viscosity of the fluid, level of the velocity. Results are interpreted in term of added mass and damping ratio on the rocking mode. In parallel of the tests program, an analytical model is developed and shows a good agreement with the experiments. Finally, for this particular geometry, analytical laws are given to estimate the modal damping due to the fluid.

KEYWORDS
Nuclear reactor internals, annular fluid-structure interactions, rocking movement, added mass, damping ratio

1. INTRODUCTION

At lower internals level of the EPR™, there is an exceptionally thin containment annulus between the core barrel and the heavy reflector which consists in two concentric shells. The ratio between the gap thickness and heavy reflector outer diameter is roughly 0,001. This annular space filled with water constitutes a fluid sheet which plays an important role on the vibrational response of lower internals. During flow-induced vibrations tests performed at reduced scale, a rocking mode of the heavy reflector corresponding to a heavy reflector motion without movement of the core barrel has been highlighted. This mode appears in dry conditions, but disappears in water (quiescent water and under flow in cold conditions). We assume that damping effects in water are large enough to suppress this mode. Literature provides some cases of study, but usually the effects of the surrounding fluid on a slender inner shell are studied only for a quiescent fluid [1-2] or for very specific boundary conditions not in line with our needs [3]. In order to verify this assumption, an additional experimental program is thus carried out. It aims at

studying the fluid-structure interactions during the rocking motion of a cylindrical shell (n=1) confined outside by a motionless shell. In more details, the effects of damping due to the fluid viscosity and fluid flow for various thicknesses of the fluid sheet will be investigated. Experimental results will be confronted to an analytical model based on Navier-Stokes equation linearization.

2. TEST FACILITIES

The experimental set-up consists in two concentric cylindrical shells made from stainless steel. The outer one is embedded by the means of clampings. The inner one is clamped at the bottom through a slender ring resulting in a cantilevered 610 mm long beam with a privileged rocking mode (n=1), e.g., Fig.1(a) for details. To study the effect of the annular thickness, four different inner shells were used (e.g., Table I). The inner shells n°1 to 3 were designed to keep the same structural mass, and as a consequence the same natural frequency in air. The shell n°4 is a modification of the shell n°2 with a re-machined outer surface reducing the outer diameter in order to increase the annular thickness. The mock-up is included in a hydraulic loop able to feed the set-up with cold (20°C) and hot (60°C) water in order to modify the fluid viscosity. The mean velocity in the annular channel can be set from 0 m/s to 6 m/s. Fluid velocity inside the inner shell can be neglected with respect to the mean velocity in the annular channel.

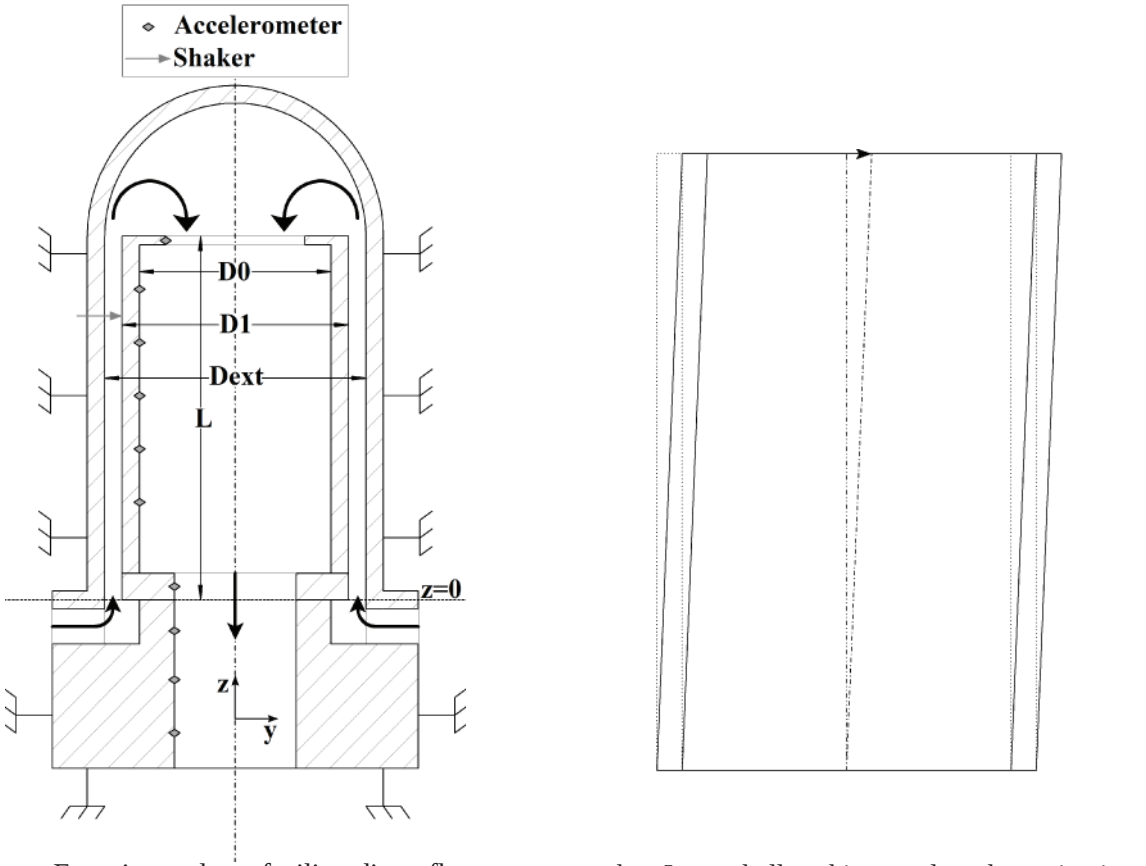

a. Experimental test facility, direct flow b. Inner shell rocking mode, schematic view

Figure 1. Experimental test facility and inner shell rocking mode

Table I. Mean annular thickness e and structural mass m_s of inner shells

Inner shell n°	e (mm)	m_s (kg)
1	0.55±0.015	60
2	2.06±0.06	61
3	4.04±0.03	61
4	10.00±0.05	41

In order to determine the system transfer function, the inner shell is equipped with accelerometers (PCB 352M201, sensitivity ~ 100 mV/g +/- 3% in the frequency range 5 Hz-10 kHz), see Fig. 1(a) for details. The excitation of the system is ensured by a shaker (PRODERA EX2060) equipped with a force sensor (KISTLER Variocomp 9601A, sensitivity ~ 120 N/V +/- 1%). The shaker is connected to the inner shell passing through the outer shell by a feedthrough seal. The shaker provide a laterally excitation in a radial direction. The accelerometers are located on the same vertical line and in the same plane than the shaker. From classical analysis of transfer functions, frequency, modal shape and modal damping (half-power bandwidth method) of the rocking mode are determined.

3. ANALYTIC MODEL

The analytic model is based on a Navier-Stokes equations linearization. The objective is to obtain fully explicit algebraic laws for the added mass and damping ratio. Thus each term is analyzed in term of order of magnitude and linearized consequently.

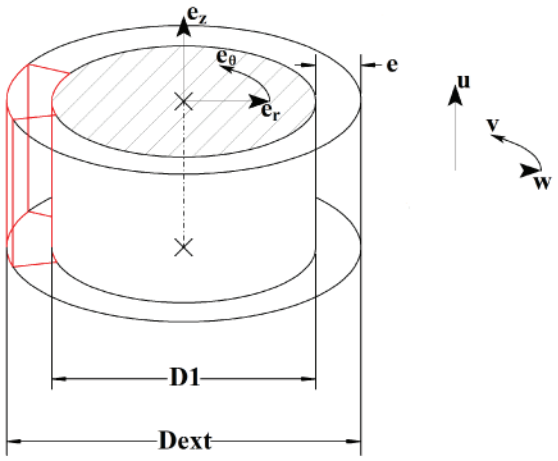

Figure 2. Coordinate system.

3.1. Fluid displacement field

Each component of the fluid displacement is divided into radial, orthoradial, axial and time contribution. The time dependence is expressed as an oscillatory contribution. The radial dependence for the othoradial and axial terms are the same considering that the annular channel aspect ratio e << R1 (close to the parallel plates problem). The general form of the velocity field is:

$$\vec{U} = \begin{cases} \dot{w}(r,\theta,z,t)\cdot\vec{e}_r = \dfrac{\partial w}{\partial t}\cdot\vec{e}_r = \dfrac{\partial\left(\phi(r)\cdot w_0(z)\cdot T(\theta)\cdot e^{i\omega t}\right)}{\partial t}\cdot\vec{e}_r \\ \dot{v}(r,\theta,z,t)\cdot\vec{e}_\theta = \dfrac{\partial v}{\partial t}\cdot\vec{e}_\theta = \dfrac{\partial\left(\gamma(r)\cdot S(z)\cdot Q(\theta)\cdot e^{i\omega t}\right)}{\partial t}\cdot\vec{e}_\theta \\ \left[V+\dot{u}(r,\theta,z,t)\right]\cdot\vec{e}_z = \left[V+\dfrac{\partial u}{\partial t}\right]\cdot\vec{e}_z = \left[V+\dfrac{\partial\left(\gamma(r)\cdot u_0(z)\cdot R(\theta)\cdot e^{i\omega t}\right)}{\partial t}\right]\cdot\vec{e}_z \end{cases} \quad (1)$$

3.2. Displacements boundary conditions

The outer shell is still, hence there is no fluid velocity on the outer boundary:

$$\vec{U}\Big|_{r=Re\,xt} = \vec{0} \quad (2)$$

The annular thickness oscillates around a stable position e, e.g., Fig.3, this oscillatory component of the thickness is defined as:

$$\text{Thickness}(\theta,z,t) = e + h(\theta,z,t) \quad (3)$$

On the inner shell boundary the continuity of the normal displacements is ensured.

$$\left(\vec{U}-\dot{\vec{X}}_{structure}\right)\bullet\vec{n} = \left(\vec{U}-\left(-\dot{h}\cdot\vec{e}_r\right)\right)\bullet\vec{n} = 0 \quad (4)$$

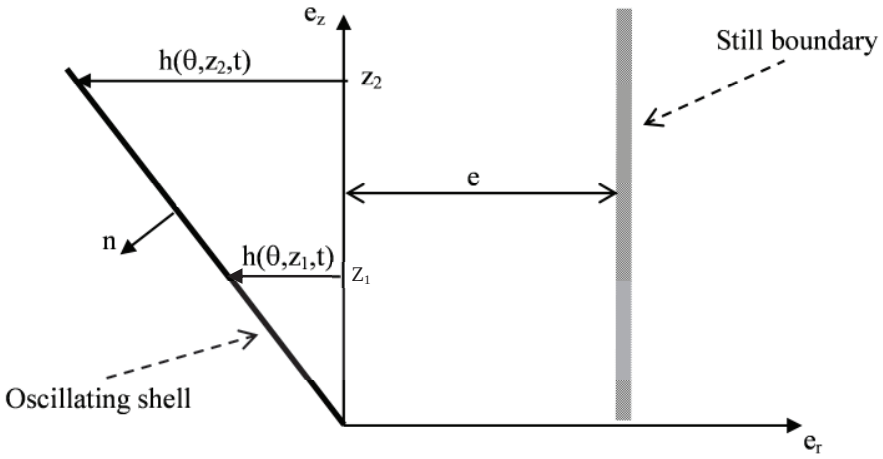

Figure 3. Boundary conditions.

According to the geometry defined in Fig. 3, the boundary condition on the inner shell can be written as:

$$\vec{U}\Big|_{r=R1} = \begin{cases} -\left(\dot{h} + V \cdot \dfrac{\partial h}{\partial z}\right) \cdot \vec{e}_r \\ 0 \cdot \vec{e}_\theta \ \left(\text{no rotation of the inner shell}\right) \\ V \cdot \vec{e}_z \end{cases} \tag{5}$$

3.3. Linearization of Navier-Stokes equations

The original form of the continuity equation is:

$$\operatorname{div}(\vec{U}) = 0 \Rightarrow \frac{1}{r} \cdot \frac{\partial\left(r \cdot \dot{w}\right)}{\partial r} + \frac{1}{r} \cdot \frac{\partial \dot{v}}{\partial \theta} + \frac{\partial\left(V + \dot{u}\right)}{\partial z} = 0 \tag{6}$$

Due to the thin gap of the fluid sheet, following hypothesis can be used:

- $h << e$
- $e << R$
- $\dot{v}(r, \theta, z, t) \approx \dot{v}(\theta, z, t) = \overline{\dot{v}}\left(\theta, z, t\right)$
- $\dot{w}(r, \theta, z, t) \approx \dot{w}(\theta, z, t) = \dot{w}\Big|_{r=R1}$

After simplification and integration on the fluid sheet thickness by taking account of (2), (5), the continuity equation becomes:

$$\boxed{i \cdot \omega \cdot \frac{\partial \overline{u}}{\partial z} + \frac{V}{e} \cdot \frac{\partial h}{\partial z} + i \cdot \omega \cdot \frac{\partial \overline{v}}{R1 \partial \theta} + i \cdot \omega \cdot \frac{h}{e} = 0} \tag{7}$$

The original form of the momentum equation is:

$$\frac{\partial \vec{U}}{\partial t} + \left(\vec{U} \bullet \vec{\nabla}\right)\left(\vec{U}\right) + \frac{1}{\rho} \cdot \vec{\nabla}\left(P + p\right) - \nu \, \tilde{\Delta}\left(\vec{U}\right) = 0 \tag{8}$$

Due to the thin gap of the fluid sheet, the following hypothesis can be used:

- $h << e$
- $e << R$
- Oscillating velocities $\left(\dot{u}, \dot{v}, \dot{w}\right)$ are small in front of the mean velocity V, thus the products of small terms are neglected
- $St << 1$
- $p(r, \theta, z, t) \approx \overline{p}(\theta, z, t)$ (thin gap approximation)

After simplification and integration by taking account of (2), (5), the momentum equation projected on $\vec{e}_z$ becomes:

$$-\rho \cdot \omega^2 \cdot \overline{u} + \rho \cdot i \cdot \omega \cdot V \cdot \frac{\partial \overline{u}}{\partial z} + \frac{\partial \overline{p}}{\partial z} + \frac{h}{e} \cdot \frac{\partial P}{\partial z} + \rho \cdot \frac{2}{e} \int_{R1}^{Re\,xt} d\tau_z dr = 0 \tag{9}$$

The viscous tensions can be expressed as below [4]:

$$\int_{R1}^{Rext} d\tau_z dr = \frac{1}{2}\cdot\frac{Cf}{4}\cdot\left(V+\bar{u}\right)^2 \tag{10}$$

The friction coefficient Cf for an annular channel can be found in references [5-6]:

- Re < 2000, $Cf = 96/Re$,
- 2000 < Re < 3000, Cf = 0.03,
- 3000 < Re < 4000, Cf = 0.04,
- Re < 4000, $Cf = 1.07\,x\,0.316\,x\,Re^{0.25}$

Applying a Taylor development on the viscous term and simplifying, equation (10) can write:

$$\underbrace{-\rho\cdot\omega^2\cdot\bar{u}}_{\text{Inertia}}+\underbrace{\rho\cdot i\cdot\omega\cdot V\cdot\frac{\partial\bar{u}}{\partial z}}_{\text{Coriolis}}+\frac{\partial\bar{p}}{\partial z}+\underbrace{\frac{h}{e}\cdot\frac{\partial P}{\partial z}}_{\text{Permanent viscous friction}}+\underbrace{Cf'\cdot\rho\cdot i\cdot\omega\cdot\frac{V}{2\cdot e}\cdot\bar{u}}_{\text{Oscilating viscous friction}}=0 \tag{11}$$

With: $-\frac{\partial P}{\partial z}=Cf\cdot\rho\frac{V^2}{4\cdot e}$ and $Cf'=Cf+\frac{1}{2}\cdot\frac{dCf}{d\,Re}\cdot Re$

Similarly, the integrated and simplified form of the momentum equation projected on $\vec{e}_\theta$ is:

$$\underbrace{-\rho\cdot\omega^2\cdot\bar{v}}_{\text{Inertia}}+\underbrace{i\cdot\rho\cdot\omega^2\cdot\bar{v}\cdot\sqrt{2\cdot S_t}}_{\text{Viscous friction}}+\underbrace{\rho\cdot i\cdot\omega\cdot V\cdot\frac{\partial\bar{v}}{\partial z}}_{\text{Coriolis}}+\frac{\partial\bar{p}}{R1\partial\theta}=0 \tag{12}$$

To solve this equations system (8), (12), (13) it's necessary to associate boundary conditions. Singular head losses have to be included. Conditions of no fluctuating flow at z = 0 and an effect of singular pressure loss linearized for the small fluctuations at z = L have been introduced giving the following boundary conditions:

$$\begin{cases}\dfrac{\partial p(r,\theta,z=0,t)}{\partial z}=0\\ p(r,\theta,z=L,t)=-i\omega^2\,K\,\rho\,V\,u(L)\end{cases} \tag{13}$$

K is the pressure loss coefficient, according to [7], K = 1 for a sudden enlargement and this value is independent of the Reynolds number Re.

The system so established is complicated to solve analytically. The strategy adopted to solve the problem is to consider independently each term representing the flow effect (viscous friction, singular pressure loss, Coriolis). This approach remains valid as far as all these terms are small (< 1) and as far as the system is now linear.

3.4. Added mass and damping ratio computation

The added mass and damping ratio are extracted from the oscillatory generalized force. The generalized force is computed from the integration of the oscillating pressure projected on the modal shape of the structure. The modal shape is assumed linear.

$$F_G = \int_{z=0}^{z=L}\int_{\theta=0}^{\theta=2\pi} \bar{p}(\theta,z,t)\cdot\frac{z}{L}\cdot dz\cdot\cos(\theta)\cdot R1\cdot d\theta = f_G\cdot e^{i\omega t} \quad (14)$$

Considering that the added mass is great compared to the structural mass due to the confinement effect, thus $m_G = m_a + m_s \approx m_a$ and the damping is small $\xi << 1$, one can write:

$$m_a = \frac{Re(f_G)}{\omega^2},\ \xi = -\frac{1}{2}\frac{Im(f_G)}{Re(f_G)} \quad (15), (16)$$

3.5. Added mass and exit pressure loss damping

Equations (11) and (12) are diminished from friction and Coriolis terms, hence:

$$\bar{u} = \left(\frac{1}{\rho\cdot\omega^2}\right)\cdot\frac{\partial\bar{p}}{\partial z},\ \bar{v} = \left(\frac{1}{\rho\cdot\omega^2}\right)\cdot\frac{\partial\bar{p}}{R1\partial\theta} \quad (17), (18)$$

Combining (17), (18) with continuity equation (7), one can write:

$$\frac{i\cdot\omega}{\rho\cdot\omega^2}\cdot\left(\frac{\partial^2\bar{p}}{\partial z^2}+\frac{\partial^2\bar{p}}{(R1\partial\theta)^2}\right)+i\cdot\omega\cdot\frac{h}{e}=0 \quad (19)$$

Internal shell vibration is assumed linear such as $h = -z/L\cos(\theta)e^{i\omega t}$. Considering boundary conditions, the oscillating pressure has then a space distribution harmonious with θ as $\bar{p}(\theta,z,t) = \bar{p}_0(z)\cdot\cos(\theta)\cdot e^{i\omega t}$ and allows to write:

$$\frac{d^2\bar{p}_0}{dz^2}-\frac{\bar{p}_0}{R1^2}-\cdot\rho\cdot\omega^2\cdot\frac{z}{e\cdot L}\cdot=0 \quad (20)$$

$\bar{p}$ is obtained by the resolution of (20) with the boundary conditions (13) and projected on the modal shape to get the generalized force:

$$f_G = \left(\pi\cdot\rho\cdot R1\cdot\omega^2\cdot\frac{L^3}{e}\right)\cdot\left(F(\alpha_0)-i\cdot K\cdot F_1(\alpha_0)\cdot V_{RL}\right) \quad (21)$$

With:
$$\begin{cases} F(\alpha) = \frac{\alpha^2}{3}+\alpha^3\left[\left[\alpha^2-1\right]\tanh\left(1/\alpha\right)+\alpha\left(1-\frac{2}{\cosh\left(1/\alpha\right)}\right)\right] \\ F_1(\alpha) = \alpha^3\left[\tanh\left(1/\alpha\right)-\alpha\left(1-\frac{1}{\cosh\left(1/\alpha\right)}\right)\right]\left[1-\frac{1}{\cosh\left(1/\alpha\right)}-\frac{1}{\alpha}\tanh\left(1/\alpha\right)\right] \end{cases}$$

The added mass is extracted from the following generalized force expression:

$$m_a = \frac{Re(f_G)}{\omega^2} = \pi \cdot \rho \cdot R1 \cdot \frac{L^3}{e} \cdot F(\alpha_0) \tag{22}$$

With a similar approach the evolution of the added mass with the filling level can be found:

$$m_a(l) = \pi \cdot \rho \cdot \frac{R1}{e} \cdot \frac{l^5}{L^2} \cdot F(\alpha) \tag{23}$$

Then the exit pressure loss damping is defined as followed:

$$\xi_{\Delta p\,exit} = -\frac{1}{2} \cdot \frac{Im(f_G)}{Re(f_G)} = \frac{K}{2} \cdot \frac{F_1(\alpha_0)}{F(\alpha_0)} \cdot V_{RL} \tag{24}$$

3.6. Friction damping

Only the contribution of the viscous friction is considered here, equations (11) and (12) thus become:

$$\bar{u} = \frac{1}{\rho \cdot \omega^2 - Cf' \cdot \rho \cdot i \cdot \omega \cdot \frac{V}{2 \cdot e}} \cdot \frac{\partial \bar{p}}{\partial z}, \bar{v} = \frac{1}{\rho \cdot \omega^2 \cdot \left[1 - i \cdot \sqrt{2 \cdot S_t}\right]} \cdot \frac{\partial \bar{p}}{R1 \partial \theta} \tag{25), (26}$$

These expressions are combined with (7), hence:

$$\frac{i \cdot \omega}{\rho \cdot \omega^2 - Cf' \cdot \rho \cdot i \cdot \omega \cdot \frac{V}{2 \cdot e}} \cdot \frac{\partial^2 \bar{p}}{\partial z^2} + \frac{i \cdot \omega}{\rho \cdot \omega^2 \cdot \left[1 - i \cdot \sqrt{2 \cdot S_t}\right]} \cdot \frac{\partial^2 \bar{p}}{(R1 \partial \theta)^2} + i \cdot \omega \cdot \frac{h}{e} = 0 \tag{27}$$

Based on h and $\bar{p}$ expressions, see §3.5, (27) is equivalent to:

$$\frac{d^2 \overline{p_0}}{dz^2} - \frac{1 - i \cdot C_f' \cdot \frac{V_{RE}}{2}}{1 - i \cdot \sqrt{2 \cdot S_t}} \cdot \frac{\overline{p_0}}{R^2} - \rho \cdot \omega^2 \left(1 - i \cdot C_f' \cdot \frac{V_{RE}}{2}\right) \cdot \frac{z}{H \cdot e} = 0 \tag{28}$$

$\bar{p}$ is obtained by the resolution of (28) with the boundary conditions (13) and projected on the modal shape to get the generalized force:

$$f_G \approx \pi \cdot \rho \cdot R1 \cdot \omega^2 \cdot \frac{L^3}{e} \cdot F(\alpha_0) \cdot \left[1 - i \cdot \left[\left(Cf' \cdot \frac{V_{RE}}{2}\right)\left(1 - \frac{g(\alpha_0)}{2}\right) + \left(g(\alpha_0) \cdot \frac{\sqrt{S_t}}{\sqrt{2}}\right)\right]\right] \tag{29}$$

With: $g(\alpha) = \alpha \frac{\frac{dF}{d\alpha}(\alpha)}{F(\alpha)}$. It results in:

$$\xi_{visc} = -\frac{1}{2}\cdot\frac{Im(f_G)}{Re(f_G)} = \left[1-\frac{g(\alpha_0)}{2}\right]\cdot C'_f\cdot\frac{V_{RE}}{4} + \frac{g(\alpha_0)}{\left(2\cdot\sqrt{2}\right)}\cdot S_t^{1/2} \quad (30)$$

3.7. Coriolis damping

Removing the friction terms in (11) and (12), one can write:

$$\bar{u} = \frac{1}{\rho\cdot\omega^2}\cdot\left(\rho\cdot i\cdot\omega\cdot V\cdot\frac{\partial\bar{u}}{\partial z} + \frac{\partial\bar{p}}{\partial z}\right),\ \bar{v} = \frac{1}{\rho\cdot\omega^2}\cdot\left(\rho\cdot i\cdot\omega\cdot V\cdot\frac{\partial\bar{v}}{\partial z} + \frac{\partial\bar{p}}{R1\partial\theta}\right) \quad (31), (32)$$

Combining the expressions above with the continuity equation (7), results in:

$$\frac{i\cdot\omega}{\rho\cdot\omega^2}\cdot\left[\rho\cdot i\cdot\omega\cdot V\cdot\left(\frac{\partial^2\bar{u}}{\partial z^2} + \frac{\partial^2\bar{v}}{R1\partial\theta\,\partial z}\right) + \frac{\partial^2\bar{p}}{\partial z^2} + \frac{\partial^2\bar{p}}{(R1\partial\theta)^2}\right] + i\cdot\omega\cdot\frac{h}{e} + \frac{V}{e}\cdot\frac{\partial h}{\partial z} = 0 \quad (33)$$

Based on h and $\bar{p}$ expressions, see §3.5, (33) can be simplified:

$$\frac{d^2\overline{p_0}}{dz^2} - \frac{\overline{p_0}}{R1^2} + 2\cdot\rho\cdot i\cdot\omega^2\cdot\frac{V_{RL}}{e} - \rho\cdot\frac{\omega^2}{e}\cdot\frac{z}{L} = 0 \quad (34)$$

$\bar{p}$ is obtained by the resolution of (34) with the boundary conditions (13) and projected on the modal shape to get the generalized force:

$$f_G = \left(\pi\cdot\rho\cdot R1\cdot\omega^2\cdot\frac{L^3}{e}\right)\cdot\left(F(\alpha_0) - i\cdot 2\cdot F_2(\alpha_0)\cdot V_{RL}\right) \quad (35)$$

With: $F_2(\alpha) = \alpha^3\cdot\left[\frac{1}{2\cdot\alpha} - \tanh\left(1/\alpha\right) + \alpha\cdot\left(1-\frac{1}{\cosh\left(1/\alpha\right)}\right)\right]$

Finally the Coriolis damping is:

$$\xi_{coriolis} = -\frac{1}{2}\cdot\frac{Im(f_G)}{Re(f_G)} = \frac{F_2(\alpha_0)}{F(\alpha_0)}\cdot V_{RH} \quad (36)$$

3.8. Total damping

The total damping is the sum of all the damping ratios:

$$\xi = \xi_{structural} + \xi_{coriolis} + \xi_{visc} + \xi_{\Delta p\ exit} \quad (37)$$

$\xi_{structural}$ is the intrinsic damping of the structure.

4. TEST RESULTS AND COMPARISON WITH THE MODEL

4.1. Dry tests

These tests are performed in order to determine the natural frequency, the modal shape and the modal damping of the rocking mode in dry conditions. As shown in Fig. 4 the modal shape is close to a linear one thanks to the slender ring. The measured structural damping is close to 1%, which is a typical value. One can note that for the inner shell n°1 (0.5 mm) the damping ratio is higher than usual, the cause of this extra damping is likely to be the thin air sheet confined between the inner and outer shell.

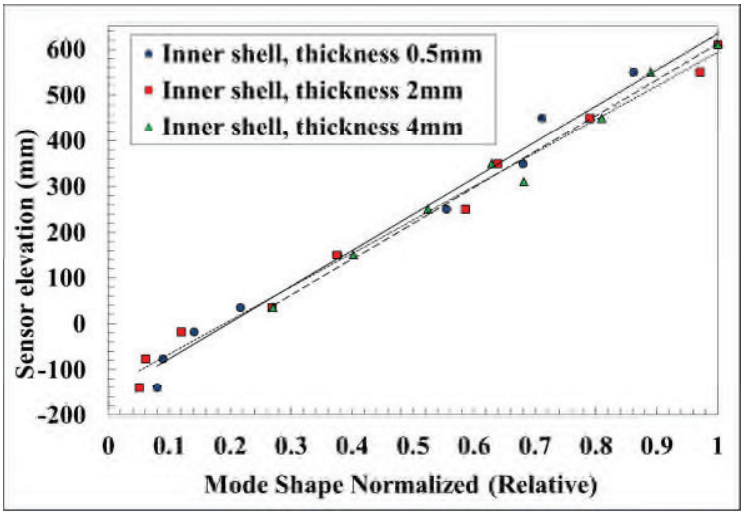

Figure 4. Inner shell rocking mode, modal shape, dry conditions.

Table II. Dry tests, natural frequencies and structural damping

Inner shell n°	Frequency (Hz)	Structural damping (%)
1	232	2.0
2	245	1.3
3	238	1.1
4	259	1.3

4.2. Quiescent water tests

The aim of the quiescent water tests is to measure the evolution of the added mass with the filling level and to determine the quiescent viscous part of the damping. The quiescent viscous part of the damping is determined by deducing the structural damping measured in dry conditions from the total damping measured in still water. It's noteworthy to mention that during the variable filling level tests the inner part of the inner shell was also filled at the same level than the annular channel, thus it has to be considered when computing the added mass. As shown in Fig. 5 and Table III the predicted added mass evolution with the filling level (23) is in a good agreement with the measurements. Moreover, Table III shows that the quiescent viscous damping follows well the simplified model developed in reference [8]. This model can be written as:

$$\xi_{\text{quiescent viscous}} = \sqrt{\frac{St}{2}} \tag{38}$$

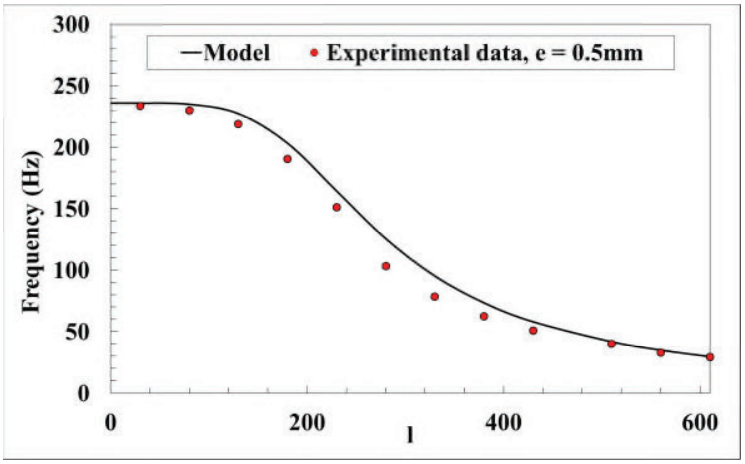

Figure 5. Evolution of the natural frequency with the filling level.

Table III. Quiescent water tests, fully filled (l=L), natural frequency and viscous damping

Inner shell n°	Rocking mode frequency (Hz)		Quiescent viscous damping (%)			
			20 °C		60 °C	
	Exp.	Model (23)	Exp.	Model (38)	Exp.	Model (38)
1	29	24	10.7	10.3	5.4	6.5
2	56	45	2.1	2.0	1.1	1.3
3	72	63	1.0	0.9	0.4	0.6
4	104	85	0.3	0.3	0.1	0.2

4.3. Flowing tests

The flowing tests allow extracting the influence of the velocity in the annulus on the damping which is also the main goal of the analytic model. The velocity homogeneous distribution in the annular channel is ensured by pressure loss measurements spread all over the circumference of the outer shell. The influence of the external flow on the added mass is negligible. Fig. 6 to Fig. 9 show the evolution of the total damping versus the mean velocity in the annular channel. In every tested configuration, the increase of the flowing velocity in the annulus results in an increase of the total damping. For the inner shell n°1 (0.5 mm), the computed total damping ratio (37) shows that the major part of it comes from the viscous contribution (30). Hence the good agreement between the model and the experience, e.g., Fig.6, confirms the performance of the model for the viscous term. The damping produced for wider annular channels is more balanced between each phenomenon. As shown on Fig. 7 to Fig. 8 the agreement between the model and the experience is still satisfying for wider annulus. However the correlation isn't quite as good as for the 0.5 mm annulus, probably because the linearization approach tends to neglect eventual cross effects and because the singular pressure loss modeling (24) is quite imperfect. Concerning the possibility to measure this coefficient, it is noteworthy to realize that it's based on an oscillatory pressure loss assumption as a way to create a model.

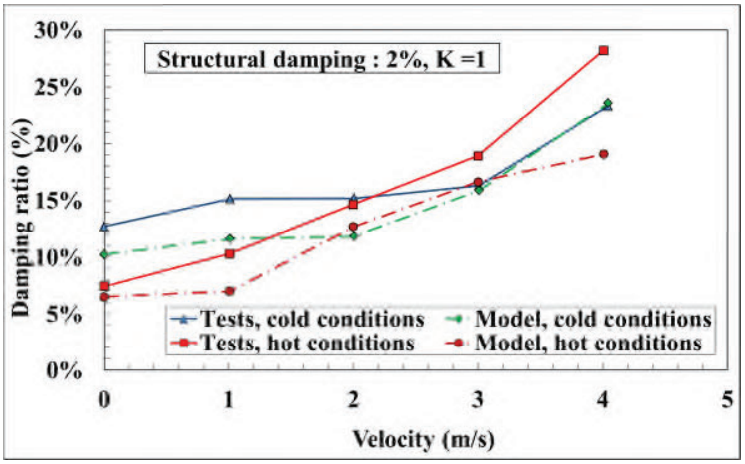

Figure 6. Flowing tests, e= 0.5 mm, damping ratio versus mean annular velocity.

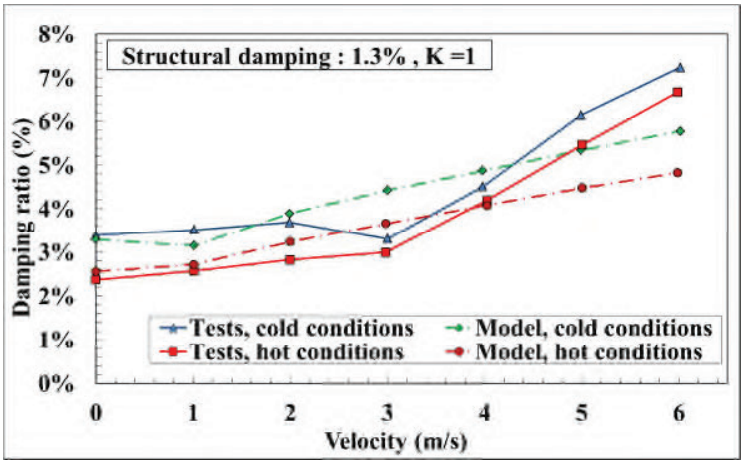

Figure 7. Flowing tests, e= 2 mm, damping ratio versus mean annular velocity.

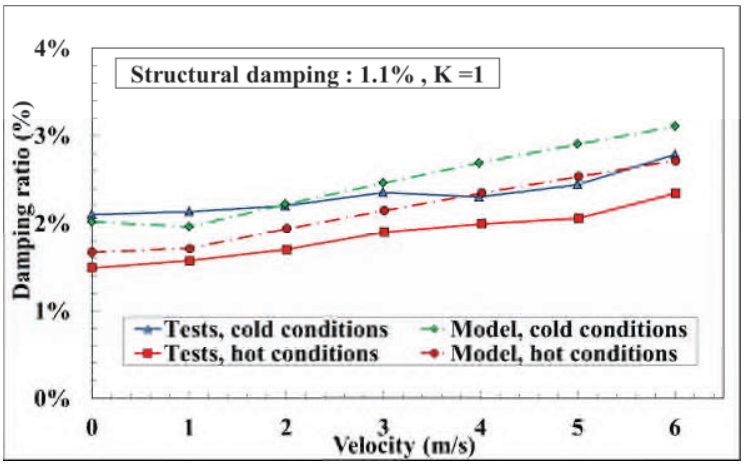

Figure 8. Flowing tests, e = 4 mm, damping ratio versus mean annular velocity.

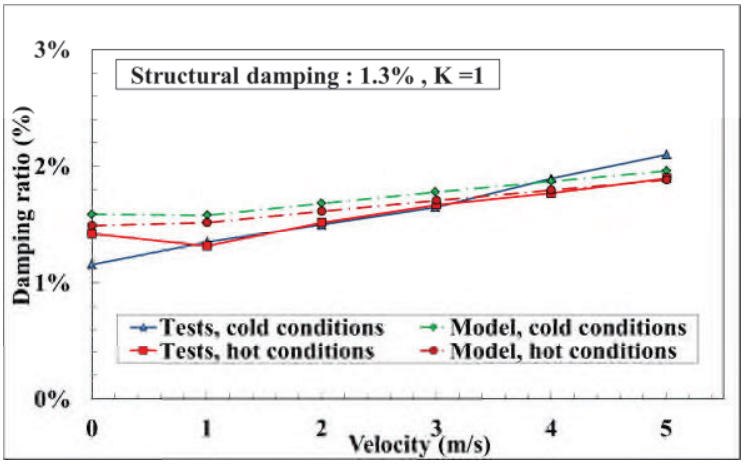

Figure 9. Flowing tests, e = 10 mm, damping ratio versus mean annular velocity

5. CONCLUSIONS

This experimental study of the inner shell rocking mode of a flowing annular channel confirms, as we assumed, that its modal damping can be important (>10%) due to fluid effects, especially when the fluid viscosity is high and the annular thickness is low. The interest of the model is on one hand to find the inertial effects which are relatively well mastered for this kind of geometry, but especially to assess the dissipative effects in the presence of flow in the fluid sheet what is rarely studied. The present attempt of modelling is what one can make of more complete by remaining in the range of the simplified descriptions of fluid-structure interactions phenomena. It contains a number of assumptions, the most questionable of which are certainly the ones concerning the treatment of boundary conditions. The experimental confrontation is globally satisfactory in terms of order of magnitude. A closer look highlights the satisfactory treatment of the viscosity. It induces a good estimation of the damping in flow in the case of the thinnest sheet, where the phenomenon of friction by viscosity is predominant. The agreement is less accurate for thicker fluid sheets. In this specific case, the various damping effects are almost equivalent. Most of the observed divergences emerge from boundary conditions and in particular from the consideration of the singular pressure loss effects.

NOMENCLATURE

D0, R0	:	Inner shell inner diameter, radius	m
D1, R1	:	Inner shell outer diameter, radius	m
Dext, Rext	:	Outer shell inner diameter, radius	m
e	:	Mean annular thickness, $e = 1/2(Dext - D1)$	m
h		Thickness fluctuation	m
L	:	Inner shell length	m
l	:	Filling level	m
V	:	Mean velocity in the annular channel	m/s
r, θ, z		Cylindrical coordinates	n/a
u, v, w	:	Fluid displacement components associated to the oscillation	m
P	:	Static permanent pressure	Pa
p	:	Static oscillatory pressure	Pa
K		Singular pressure loss coefficient	n/a

α	:	Non dimensional filling level, $\alpha = R1/l$	n/a
α_0	:	Non dimensional inner shell height, $\alpha_0 = R1/L$	n/a
m_s	:	Structural mass	kg
m_a	:	Added mass	kg
m_{tot}	:	Total mass, $m_{tot} = m_a + m_s$	kg
F_G	:	Generalized oscillatory force	N
ξ	:	Damping ratio	n/a
V_{RL}	:	Non dimensional velocity, $V_{RL} = V/(\omega L)$	n/a
V_{RE}	:	Non dimensional velocity, $V_{RE} = V/(\omega e)$	n/a
Cf	:	Friction coefficient	n/a
Cf'	:	Modified friction coefficient	n/a
ρ	:	Fluid density	Kg/m^3
ν	:	Fluid kinematic viscosity	$m^2.s$
ω	:	System pulsation	Rad/s
Re	:	Reynolds number, $Re = (V2e)/\nu$	n/a
St	:	Stokes number, $St = \nu/(\omega e^2)$	n/a
$\vec{n}$	:	Normal unitary vector oriented towards the fluid	n/a
$\dot{\vec{X}}_{structure}$	:	Structure velocity vector	m/s

REFERENCES

1. W.G. Sim, "Damping Forces of Vibrating Cylinder in Confined Viscous Fluid by a Simplified Analytic Method," *KSME International Journal* **8** (1), pp. 43-51 (1994).
2. W.G. Sim, Y.C. Cho, "Study of Unsteady Fluid-Dynamic Forces acting on a flexible cylinder in a concentric annulus," *KSME International Journal* **7** (2), pp. 144-157 (1993).
3. E. Ohlmer, S. Russo, R. Schwemmle, "Investigation of an analytical model for parallel flow induced rod vibrations," *Nuclear Engineering and Design* **22**, pp. 272-289 (1972).
4. G. Porcher, "Contribution à l'étude des instabilités fluides-élastiques des structures tubulaires sous écoulement axial confiné," PhD thesis, Paris VI University, (1994)
5. I.E. Idelchik, *Handbook of Hydraulic resistance 3rd Edition*, Chapter 2, CRC Press, (1994).
6. W.M. Rohsenow, J.P. Hartnett, E.N. Ganic, *Handbook of heat transfer fundamentals 2nd Edition*, Chapter 7, pp. 46-52, Mc Graw-Hill, (1985).
7. I.E. Idelchik, *Handbook of Hydraulic resistance 3rd Edition*, Chapter 4, CRC Press, (1994).
8. R.J. Gibert, *Vibration des structures*, pp. 368-376, Editions Eyrolles, Paris, (1988).